Photoinduced correlated electron dynamics in a two-leg ladder Hubbard system

Hiroshi Hashimoto and Sumio Ishihara
Department of Physics, Tohoku University, Sendai 980-8578, Japan
and CREST-JST, Sendai 980-8578, Japan

(Received 1 November 2015; revised manuscript received 1 April 2016; published 22 April 2016)

Photoinduced carrier dynamics in a correlated electron system on a coupled two-leg ladder lattice are studied. The two-leg ladder Hubbard model is analyzed utilizing the exact diagonalization method based on the Lanczos algorithm in finite-size clusters. In order to reveal the transient carrier dynamics after photoirradiation, we calculate the low-energy components of the hole kinetic energy, the pair-field correlation function, the optical conductivity spectra, and other characteristics. It is shown that the photoinduced metallic-like state appears in a half-filled Mott insulating state, while the low-energy carrier motion is suppressed by photoirradiation in the case of hole-doped metallic states. These photoinduced changes in the electron dynamics are associated with changes in the carrier-pair coherence; they are not attributed to a naive thermalization, and are associated with a ladder-lattice effect instead. Based on the numerical results, optical control of hole pairs using double-pulse pumping is demonstrated. Implications for recent optical pump-probe experiments are presented.

DOI: 10.1103/PhysRevB.93.165133

I. INTRODUCTION

Optical manipulations of macroscopic phenomena in solids have recently become very attractive research subjects in the field of condensed matter physics [1,2]. Techniques for the ultrafast control of magnetism [3,4], ferroelectricity [5,6], electrical conductivity [7–14], and superconductivity [15,16] have been examined for a wide variety of materials, utilizing recently developed laser-pulse technology. Strongly correlated electron systems, such as transition-metal oxides, organic molecular solids, and rare-earth compounds, in which a number of degrees of freedom are entangled with each other under strong electron-electron and electron-lattice interactions, are plausible candidate materials for the application of such control techniques. Observations of transient changes in macroscopic quantities and elucidation of the corresponding microscopic mechanisms are desired for both improved fundamental understanding and practical applications.

Low-dimensional correlated electron systems are attractive targets for the realization of ultrafast optical control of electronic states. Quasi one- and two-dimensional cuprate oxides [7,10,11,15–19], halogen-bridged complexes [8,12], and quasi two-dimensional molecular solids [13,14] are of examples of such systems, because of their rich variety of equilibrium states and simple lattice structures. From the theoretical viewpoints, transient electron dynamics have been examined numerically and analytically in the one- and two-dimensional Hubbard [20–23] and $t-J$ [18,19] models, which are accepted as minimal models for low-dimensional correlated electron systems.

Correlated electrons on a ladder lattice are recognized to constitute an intermediate configuration between one- and two-dimensional systems. The superconductivity observed in the two-leg ladder cuprates, $Sr_{14-x}Ca_xCu_{24}O_{41}$, suggests unique electronic structures on a ladder lattice. In these materials, the insulating state associated with the charge order at $x = 0$ is transformed into a metallic state through substitution of Ca for Sr, and superconductivity appears under high pressure [24–27]. Short-range singlet spin correlation and the spin excitation gap have attracted considerable attention owing to the superconductivity caused by the doping of holes into the ladders [28]. A number of theoretical examinations of equilibrium electric and magnetic structures, as well as investigations of doublon-holon dynamics, have been performed to date, for both the two-leg ladder Hubbard and $t-J$ models [29–36]. Recently, the photoinduced transient states in the insulating ($x = 0$) and metallic ($x = 10$) two-leg ladder cuprates were examined utilizing the ultrafast optical pump-probe method [37–39]. Such transient optical measurements provide indications of the unique spin and charge dynamics of these materials, as well as their influence on the superconductivity of two-leg ladder cuprates.

In this paper, the photoinduced carrier dynamics in a correlated electron system on a two-leg ladder lattice are studied. The two-leg ladder Hubbard model is analyzed utilizing the exact-diagonalization method, based on the Lanczos algorithm in finite-size clusters. In order to reveal the transient dynamics, we calculate the low-energy components of the kinetic energy, the pair-field correlation function, the optical conductivity spectra, and other characteristics as functions of time. It is found that the low-energy carrier dynamics in the metallic states are distinguishable from those in the insulating states; the photoinduced metallic-like state appears at the half-filled Mott insulating state, while the low-energy carrier motion is suppressed by photoirradiation in the hole-doped metallic states. These photoinduced changes in the dynamics are associated with the changes in the carrier pair coherence. Based on the calculated results, optical control of the hole pairs through use of double-pulse pumping is demonstrated. Implications for recent optical pump-probe experiments are also presented.

In Sec. II, the theoretical model and the numerical calculation method are introduced. In Sec. III A, numerical results for the photoinduced carrier dynamics are presented. In Sec. III B, numerical demonstrations of the photocontrol carrier dynamics obtained utilizing the double-pulse pumping are shown. Section IV is devoted to a discussion and summary.

II. MODEL AND METHOD

The Hubbard model on a two-leg ladder lattice is defined by

$$\mathcal{H} = -\sum_{\langle ij\rangle\alpha\sigma}(tc^{\dagger}_{i\alpha\sigma}c_{j\alpha\sigma} + \text{H.c.}) - \sum_{i\sigma}(t' c^{\dagger}_{i1\sigma}c_{i2\sigma} + \text{H.c.}) + U\sum_{i\alpha} n_{i\alpha\uparrow}n_{i\alpha\downarrow}, \quad (1)$$

where $c^{\dagger}_{i\alpha\sigma}$ and $c_{i\alpha\sigma}$ are the creation and annihilation operators for an electron at the ith rung and the right ($\alpha = 1$) or left ($\alpha = 2$) leg with spin $\sigma(=\uparrow,\downarrow)$, and $n_{i\alpha\sigma} = c^{\dagger}_{i\alpha\sigma}c_{i\alpha\sigma}$ is the number operator. The first and second terms represent the electron hopping along the leg and rung in the two-leg ladder lattice, respectively, while the third term describes the on-site Coulomb interaction. The $\langle ij\rangle$ symbol represents the nearest-neighbor ij pair along a leg. We introduce the anisotropy of the hopping integral as $r_t = t'/t$, which is almost equal to 1 for ladder cuprates. The model with $r_t = 1$ has been analyzed both intensively and extensively since the discovery of superconductivity in ladder cuprates [29,34,40–45]. Hence, it has been found that a Mott insulator at half filling, where both the spin and charge gaps exist, is transformed via doping into a correlated metal in which the spin gap remains. Long-range pair correlation is developed in weakly doped systems. The spin and charge excitation spectra and the transient holon-doublon dynamics have also been examined using numerical simulations. The same model with r_t removed from 1 has also been studied, both numerically and analytically. Note that both the spin gap and the pair correlation in the weakly doped system tend to disappear as r_t decreases from 1.

The photoinduced dynamics are examined by introducing the pump-pulse photons in the first term in Eq. (1) as the Peierls phase given by

$$t \to te^{iA(\tau)}, \quad (2)$$

where the lattice constant, light velocity, and elementary charge are taken to be units, and the light polarization is parallel to the leg direction. The vector potential of the pump-photon pulse at time τ is taken to have a Gaussian form, where

$$A(\tau) = A_p e^{-\tau^2/(2\gamma_p^2)}\cos\omega_p\tau, \quad (3)$$

with amplitude A_p, frequency ω_p, and pulse width γ_p. The center of the pump-photon pulse is located at $\tau = 0$.

The electronic states before and after the photon pumping are calculated using the exact-diagonalization method based on the Lanczos algorithm. The time evolutions of the wave function under the time-dependent Hamiltonian are calculated as [46,47]

$$|\Psi(\tau+\delta\tau)\rangle = e^{-i\mathcal{H}(\tau)\delta\tau}|\Psi(\tau)\rangle, = \sum_{i}^{M} e^{-i\varepsilon_i\delta\tau}|\phi_i\rangle\langle\phi_i|\Psi(\tau)\rangle, \quad (4)$$

where $|\phi_i\rangle$ and ε_i are the eigenstate and the eigenenergy in the order-M Krylov subspace in the Lanczos process, respectively, $\delta\tau$ is a time step, and $\mathcal{H}(\tau)$ is the time-dependent Hamiltonian, where the pump pulse is introduced using Eq. (2). For the majority of the numerical calculations in this study, we choose $M = 15$ and $\delta\tau = 0.01/t$, which yield results with sufficiently high accuracy. We adopt finite-size clusters of N ($=2\times N/2$) sites, up to $N = 14$, where periodic- and open-boundary conditions are imposed along the leg. A cluster of $N = 16$ is also adopted, in order to examine the size dependence of the ground state and the optical spectra. We qualitatively confirm that the numerical results presented in Sec. III are robust, by changing N and the boundary conditions. Detailed results for several N values are presented in Figs. 2 and 6(b), and almost all the numerical results presented in Sec. III are calculated for a cluster with $N = 12$.

All the energy and time parameters in the numerical calculations are given in units of t and $1/t$, respectively, which correspond to approximately 0.5 eV and 8 fs, respectively, in the ladder cuprates. In the majority of the calculations, we employ $U/t = 6$ and $\gamma_p t = 5$. The hole density measured from the half filling is denoted $x_h(\equiv 1 - N_e/N)$, where N_e is the number of electrons.

III. RESULTS

In this section, the transient electronic states after the photon pumping are studied. The ground states before the photon pumping are studied by calculating the spin-gap energy, the holon-binding energy, the optical conductivity spectra, the one-particle excitation spectra, and other characteristics. The majority of the results are consistent with the previous calculations for the two-leg ladder Hubbard models [29–31]. In Fig. 1, the optical conductivity spectra before pumping at half filling ($x_h = 0$) and away from half filling are shown. The optical gap at half filling collapses as a result of hole doping. Further, a sharp low-energy peak in the vicinity of $\omega/t = 0.5$, which corresponds to the Drude component, appears. We have confirmed that the energy of this peak decreases with increasing cluster size up to $N = 16$ (not shown in this figure). Thus, the finite, but small, energy of the "Drude" peak is due to the finite size effects in the open boundary condition. The ω_p are tuned to the optical gap energy in the half-filling case, and to

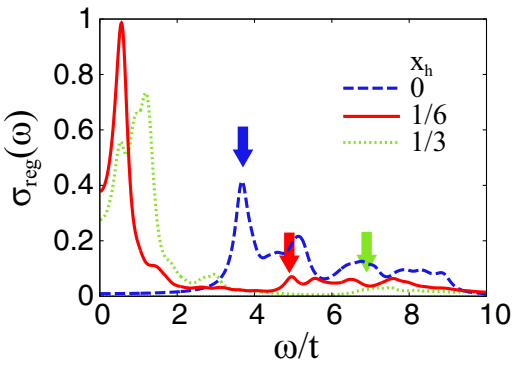

FIG. 1. Optical conductivity spectra before photon pumping. The dashed, solid, and dotted curves represent the spectra at $x_h = 0$ (half filling), 1/6, and 1/3, respectively. A finite size cluster of $N = 12$ sites with an open boundary condition is adopted. The parameter values are chosen to be $U/t = 6$ and $t'/t = 1$. The bold arrows represent the pump-photon energies adopted in the numerical calculations of the real-time photoinduced dynamics.

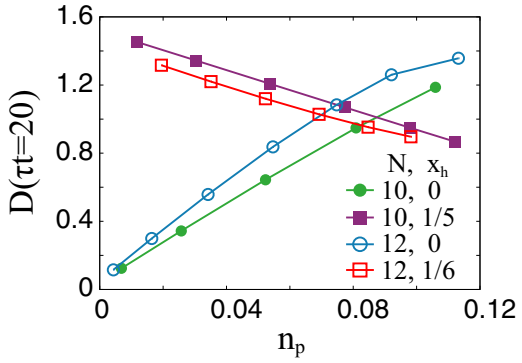

FIG. 2. Low-energy weights of optical conductivity spectra after photoirradiation as functions of absorbed photon density n_p. Results for the insulating and hole-doped cases with $N = 10$ and 12 are shown.

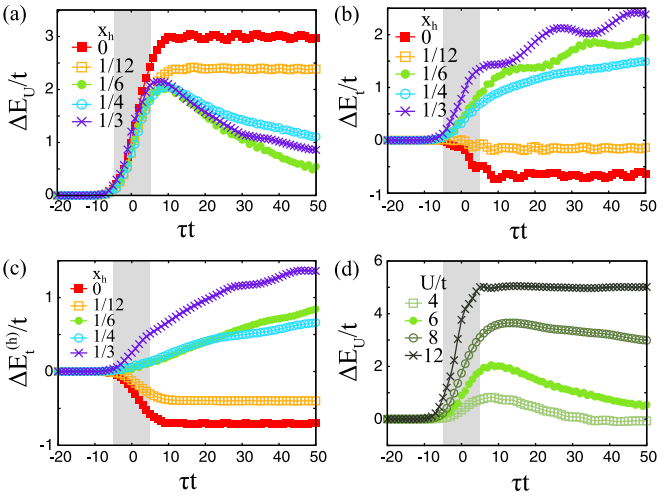

FIG. 3. (a)–(c) Increments of several energies for several hole densities. The Coulomb-interaction energy (E_U), the kinetic energy (E_t), and the kinetic energy for the low-energy hole motions ($E_t^{(h)}$) are plotted. The Coulomb interaction parameter is chosen to be $U/t = 6$. (d) Time dependences of E_U at $x_h = 1/6$ for several values of U. A finite size cluster with $N = 12$ sites under an open boundary condition is adopted. The parameter value is chosen to be $t'/t = 1$. The shaded areas represent the time interval during which the pump pulse is introduced.

the energy of the remnant gap in the hole-doped metallic state, as shown by the bold arrows in Fig. 1. We define the absorbed photon density as $n_p(\tau) = [E(\tau) - E_0]/(N\omega_p)$, where $E(\tau)$ is the total energy at time τ and $E_0 = E(\tau \ll 0)$. This measures the weight of the photoexcited-state wave function relative to that of the ground state. The numerical values of A_p are chosen in order to satisfy the condition $n_p(\tau \gg \gamma_p) \sim 0.05$, which is comparable to the absorbed photon densities in pump-probe experiments for systems in which the photoinduced phase transition emerges [8,9,11,37–39]. In Fig. 2, the low-energy weights of the optical conductivity spectra after photon pumping at $\tau t = 20$ are presented as functions of n_p [note that a definition will be given in Eq. (9)]. As will be explained in greater detail in Sec. III A, the integrated spectral weight D increases and decreases under the influence of photoirradiation in the insulating and hole-doped systems, respectively (see Fig. 4). It is worth noting that D varies smoothly as a function of n_p up to approximately 0.12 (corresponding to the strong-excitation case) in both the $N = 10$ and 12 clusters, and does not exhibit any abrupt changes at a certain value of n_p. That is, the photoinduced phenomena introduced in this section appear commonly for a wide range of A_p within the present numerical calculations.

A. Photoinduced change in carrier dynamics

First, we show the photoinduced changes in the carrier dynamics. In order to measure the low-energy dynamics of the carriers, the projected kinetic-energy expectations are introduced as [48]

$$E_t^{(h)} = -t \sum_{\langle ij\rangle\alpha\sigma} \left\langle P_{ij\alpha\bar{\sigma}}^{(h)} c_{i\alpha\sigma}^{\dagger} c_{j\alpha\sigma} P_{ij\alpha\bar{\sigma}}^{(h)} + \text{H.c.} \right\rangle, \tag{5}$$

and

$$E_t^{(d)} = -t \sum_{\langle ij\rangle\alpha\sigma} \left\langle P_{ij\alpha\bar{\sigma}}^{(d)} c_{i\alpha\sigma}^{\dagger} c_{j\alpha\sigma} P_{ij\alpha\bar{\sigma}}^{(d)} + \text{H.c.} \right\rangle, \tag{6}$$

where $\bar{\sigma} = \uparrow(\downarrow)$ for $\sigma = \downarrow(\uparrow)$. We define the projection operators as $P_{ij\alpha\sigma}^{(h)} = (1 - n_{i\alpha\sigma})(1 - n_{j\alpha\sigma})$ and $P_{ij\alpha\sigma}^{(d)} = n_{i\alpha\sigma} n_{j\alpha\sigma}$, which project onto the states in which both the i and j sites are unoccupied and occupied by electrons with σ, respectively. The projected kinetic energies $E_t^{(h)}$ and $E_t^{(d)}$ measure the kinetic energies of holes and doublons along the leg, respectively, where the number of double occupancies are unchanged, for example, $|(\uparrow)_i\rangle \rightarrow |(\uparrow)_j\rangle$ and $|(\uparrow\downarrow)_i(\downarrow)_j\rangle \rightarrow |(\downarrow)_i(\uparrow\downarrow)_j\rangle$.

In Fig. 3, several components of the energies are plotted as functions of time. The Coulomb interaction energy (E_U) and the kinetic energy (E_t) are defined as the expectation values of the third and first terms in Eq. (1), respectively. We define the energy differences as $\Delta E_U = E_U(\tau) - E_U(\tau \ll 0)$ and others. As shown in Fig. 3(a), E_U increases in response to photon pumping for all values of x_h, which implies that the number of doubly occupied sites increases. The time dependence of E_U after photon pumping is strongly dependent on x_h: large E_U is maintained at half filling, whereas this energy gradually decreases with time in the case of hole doping. The reductions in E_U imply recombinations of the photogenerated doublons and holons, with the excess E_U due to the photon pumping being transferred into E_t. In the vicinity of the half filling, no channels exist through which the large excess E_U is released. This is shown clearly in Fig. 3(d), where E_U at $x_h = 1/6$ is plotted for several values of U. Reduction of E_U is observed for small U. The lifetimes of the photogenerated doublons and holons are prolonged by increasing U, which is suggested to be $\sim e^{\alpha U}$ with a positive constant α in Ref. [49]. The numerical results of E_t and $E_t^{(h)}$ are presented in Figs. 3(b) and 3(c), respectively. Note that $E_t^{(h)} + E_t^{(d)}$ (not shown) exhibit similar behavior to $E_t^{(h)}$. At half filling, both E_t and $E_t^{(h)}$ decrease, implying increment of the carrier motion through photon pumping. Opposite changes can be seen in the hole-doped cases where both E_t and $E_t^{(h)}$ increase. That is, the carrier motions are suppressed by photon pumping.

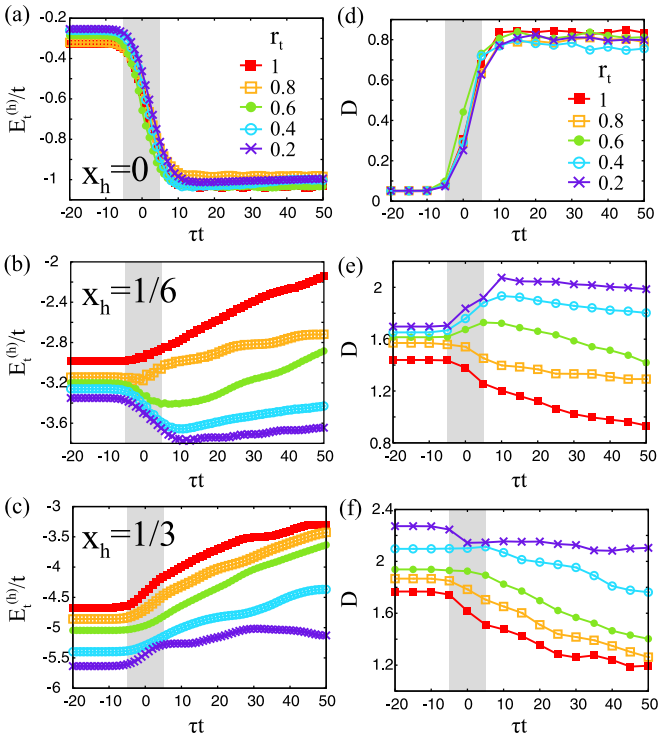

FIG. 4. (a)–(c) Kinetic energies of low-energy hole motions for several values of t'/t. (d)–(f) Low-energy weights of optical conductivity spectra for several values of t'/t. The hole densities are chosen to be $x_h = 0$ in (a) and (d), 1/6 in (b) and (e), and 1/3 in (c) and (f). A finite size cluster of $N = 12$ sites with an open boundary condition is adopted. The parameter value is chosen to be $U/t = 6$. The shaded areas represent the time interval at which the pump pulse is introduced.

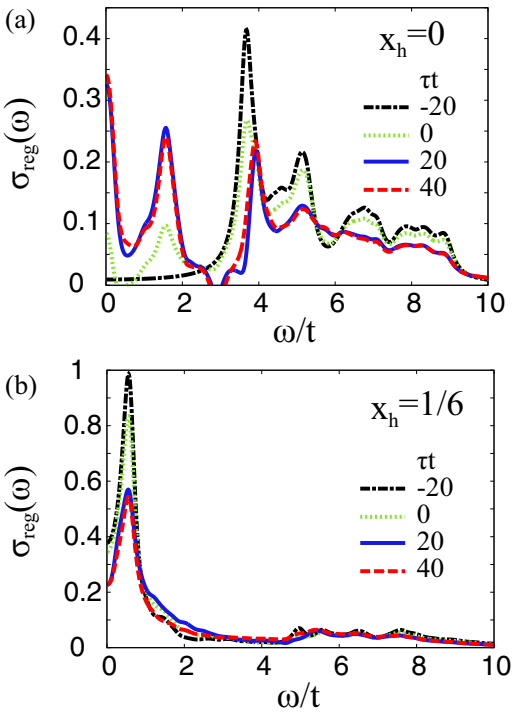

FIG. 5. Optical conductivity spectra for several times at (a) $x_h = 0$ and (b) 1/6. A finite size cluster of $N = 12$ sites with an open boundary condition is adopted. The parameter values are chosen to be $U/t = 6$ and $t'/t = 1$.

Let us focus on the photoinduced dynamics of the low-energy carrier motion. In Figs. 4(a)–4(c), the transient kinetic energies for the low-energy hole motion, $E_t^{(h)}$, are presented for several values of $r_t = t'/t$. At half filling [Fig. 4(a)], $|E_t^{(h)}|$ increases in response to the photon pumping for all values of t'/t. Remarkable t'/t dependence is apparent for the hole-doped cases of $x_h = 1/6$ [see Fig. 4(b)]. Monotonic reduction of $|E_t^{(h)}|$ after photon pumping is observed in the vicinity of $r_t = 1$. For the two weakly coupled chains corresponding to small r_t, $|E_t^{(h)}|$ increases in response to the photon pumping, similar to the results at half filling. The reductions of $|E_t^{(h)}|$ are more pronounced in $x_h = 1/3$, as shown in Fig. 4(c). Therefore, the two-leg ladder lattice plays an essential role in the suppression of the low-energy carrier dynamics induced by the photon pumping. Qualitatively $E_t^{(h)}$ behavior is confirmed in the calculations, in which the cluster sizes are $N = 5 \times 2$ to 7×2 with periodic and open boundary conditions, and U/t is chosen to be 6 and 8.

The carrier dynamics after photon pumping are also examined by calculating the transient excitation spectra. The transient optical responses are simulated using the formula based on the linear response theory, where the wave functions at time τ are used. This approach has been widely applied in order to examine the transient electronic structures in correlated electron systems [50,51], and its validity has been confirmed in Ref. [52]. The regular part of the optical conductivity spectrum is given by

$$\sigma_{\rm reg}(\omega) = -\frac{1}{N\omega}{\rm Im}\chi(\omega), \tag{7}$$

with

$$\chi(\omega) = -\sum_{mn}\left(\frac{\langle\Psi(\tau)|\phi_m\rangle\langle\phi_m|j|\phi_n\rangle\langle\phi_n|j|\Psi(\tau)\rangle}{\omega-\varepsilon_m+\varepsilon_n+i\eta} - \frac{\langle\Psi(\tau)|j|\phi_n\rangle\langle\phi_n|j|\phi_m\rangle\langle\phi_m|\Psi(\tau)\rangle}{\omega-\varepsilon_n+\varepsilon_m+i\eta}\right), \tag{8}$$

where we introduce the current operator along the leg defined by $j = it\sum_{i\alpha\sigma} c^\dagger_{i\alpha\sigma}c_{i+1\alpha\sigma} + {\rm H.c.}$ and a small positive constant η. The calculated optical conductivity spectra at $x_h = 0$ and 1/6 are shown in Figs. 5(a) and 5(b), respectively. At half filling, new peaks appear inside the optical gap in response to the photon pumping and grow with time. This is consistent with the $E_t^{(h)}$ results shown in Fig. 3(b). This change in the optical conductivity spectra implies emergence of the photoinduced metallic-like state in a Mott insulator.

On the other hand, in the hole-doped case, a sharp low-energy peak observed before pumping is diminished immediately after the photon pumping, and its intensity decreases with time. Weak changes are apparent in the high-energy excitation spectra, which are identified as remnants of the Mott gap excitations. We note that the negative values around $\omega/t = 3$ in Fig. 5(a) are attributable to the optical emission from the photoexcited states.

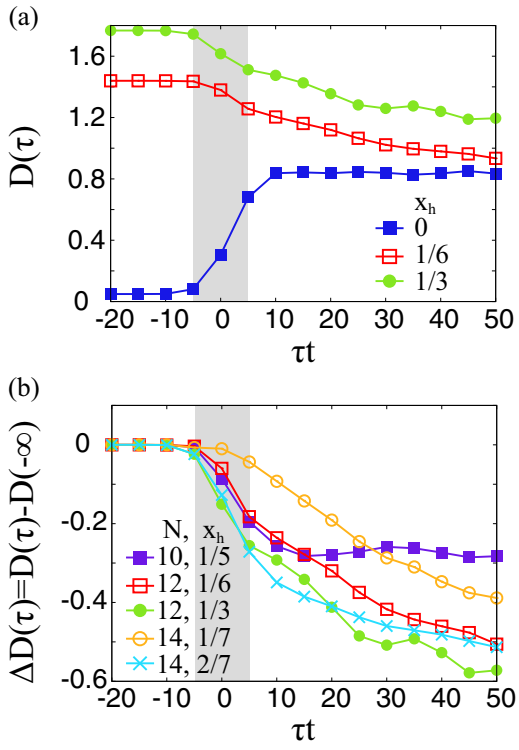

FIG. 6. (a) Time dependences of low-energy weights of optical conductivity spectra (D) for several hole densities. A finite size cluster of $N = 12$ sites with an open boundary condition is adopted. (b) Changes in low-energy weights of optical conductivity spectra for several cluster sizes and hole densities in hole-doped cases. $(N,x_h) = (10,1/5)$, $(12,1/6)$, $(12,1/3)$, $(14,1/7)$, and $(14,2/7)$. The parameter values are chosen to be $U/t = 6$, $t'/t = 1$, and $\omega_c/t = 2$. The shaded areas represent the time interval at which the pump pulse is introduced.

In order to examine the photoinduced changes in the low-energy spectral weight, we define the integrated spectral weight [53,54]

$$D = -\frac{\pi E_t}{N} - 2\int_{\omega_c}^{\infty} d\omega\, \sigma_{\rm reg}(\omega), \tag{9}$$

in the calculations with the open boundary condition, where ω_c is the cutoff energy. In Fig. 6(a), the D values are shown for several hole densities. We choose $\omega_c/t = 2$, and do not observe any qualitative differences from the results with $1 \lesssim \omega_c/t \lesssim 3$. The increase in D from zero at half filling implies the appearance of photogenerated metallic-like carrier motions. Contrasting behavior is observed for $x_h = 1/6$ and $1/3$; that is, D is reduced after photon pumping. The low-energy intensities decrease continuously, at least up to $\tau = 50/t$. As shown in Fig. 6(b), the characteristics of the hole-doped cases, i.e., reduction of D by photoirradiation, are observed for a wide range of cluster sizes and hole densities. That is, this result is made robust by changing the cluster size and the parameter values. We confirm that the reduction of D monotonically increases with A_p, and is qualitatively insensitive to the parameter values of the photon energy between $4.9 \lesssim \omega_p/t \lesssim 7.5$ in $(N,x_h) = (12,1/6)$. The low-energy spectral weights for several x_h and $r_t = t'/t$ are summarized in Figs. 4(d)–4(f). The results are qualitatively similar to the kinetic energies for the low-energy hole motion shown in Figs. 4(a)–4(c).

Photoinduced changes in the electronic structures are directly observed by calculating the one-particle excitation spectra. We calculate the transient electronic density of states (DOS), employing the wave function at time τ. This is given by

$$\rho^{\gtrless}(\omega) = \frac{1}{N}\sum_{\boldsymbol{k}} A^{\gtrless}(\boldsymbol{k},\omega), \tag{10}$$

where $\rho^{>}(\omega)$ and $\rho^{<}(\omega)$ are the DOS for the electron and hole parts, respectively, and are given by the one-particle excitation spectra defined by

$$A^{<}(\boldsymbol{k},\omega) = -\frac{1}{\pi}{\rm Im}\sum_{mn}\sum_{\alpha\sigma} \times \frac{\langle\Psi(\tau)|\phi_m\rangle\langle\phi_m|c_{\boldsymbol{k}\alpha\sigma}|\phi_n\rangle\langle\phi_n|c^{\dagger}_{\boldsymbol{k}\alpha\sigma}|\Psi(\tau)\rangle}{\omega - \varepsilon_n + \varepsilon_m + i\eta}, \tag{11}$$

and

$$A^{>}(\boldsymbol{k},\omega) = -\frac{1}{\pi}{\rm Im}\sum_{mn}\sum_{\alpha\sigma} \times \frac{\langle\Psi(\tau)|c^{\dagger}_{\boldsymbol{k}\alpha\sigma}|\phi_n\rangle\langle\phi_n|c_{\boldsymbol{k}\alpha\sigma}|\phi_m\rangle\langle\phi_m|\Psi(\tau)\rangle}{\omega - \varepsilon_m + \varepsilon_n + i\eta}. \tag{12}$$

The calculated DOS and one-particle excitation spectra are shown in Fig. 7. We assign the x and y axes parallel to the leg and rung directions, respectively. In the isotropic ladder lattice [Fig. 7(a)], the sharp peak in the vicinity of the Fermi level (FL) before pumping is attributed to the two quasiparticle bands originating from the bonding ($k_y = 0$) and antibonding ($k_y = \pi$) bands [31], which cut the FL at approximately $k_x = 0.6\pi$ and 0.3π, respectively [see Figs. 7(c) and 7(d)]. After pumping, as shown in Figs. 7(a), 7(e), and 7(f), the sharp quasiparticle peaks are more widely spread and have merged into incoherent parts. Remarkable changes in the high-energy structure are not apparent, although the electronic and hole parts are distributed to the high- and low- energy regions, respectively. On the other hand, at $r_t = t'/t = 0.2$, i.e., the weakly coupled chains case, the sharp peak around the FL before pumping remains and shifts toward the low-energy region after the photon pumping. In the numerical calculation shown in Fig. 7(b), A_p is set to a value in which n_p is taken to be approximately 0.08, in order to demonstrate the characteristics clearly. The differences between the results for $r_t = 1$ and 0.2 shown above are consistent with the r_t dependence of the low-energy E_t as well as the low-energy weight of the optical conductivity spectra shown in Fig. 4.

Finally, we show the paring properties of the charge carriers and the photon pumping effect [29,30,32]. We introduce the pair-field correlation function between sites i and j, which is defined by

$$P(|i-j|) = \langle\Psi(\tau)|(\Delta_j^{\dagger}\Delta_i + {\rm H.c.})|\Psi(\tau)\rangle, \tag{13}$$

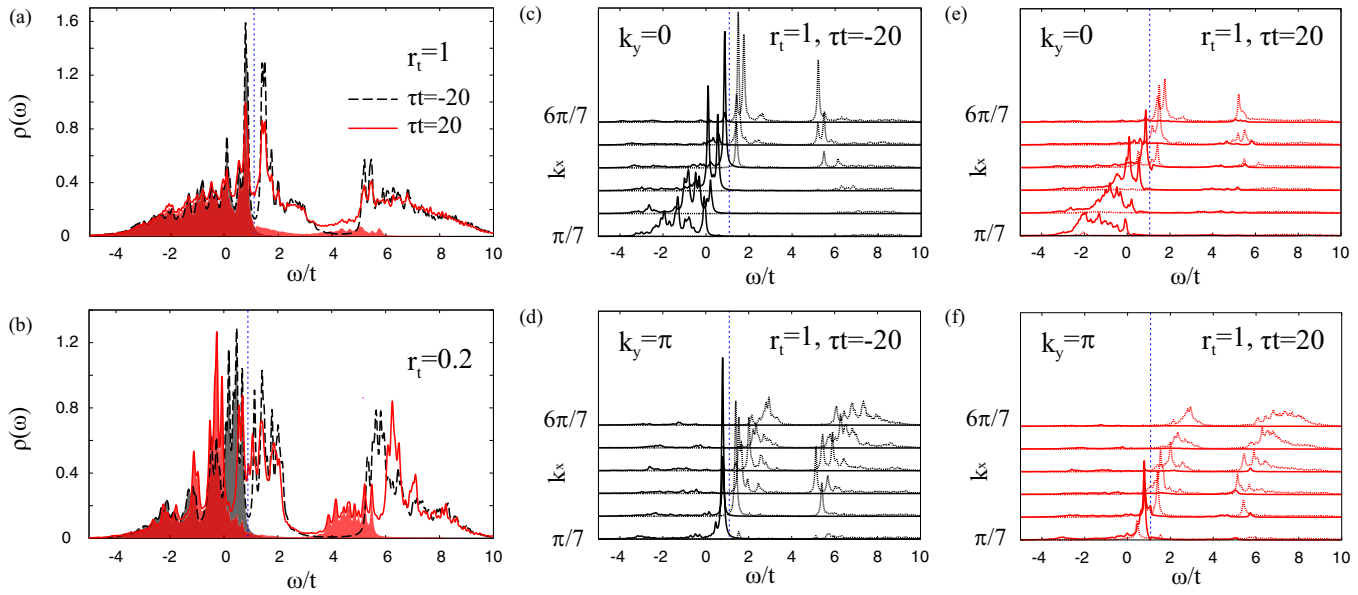

FIG. 7. (a) One-particle DOS at $r_t = 1$ and (b) those at $r_t = 0.2$ before ($\tau t = -20$) and after ($\tau t = 20$) pumping. The dashed and solid lines represent the total DOS $[\rho^<(\omega) + \rho^>(\omega)]$ before and after pumping, respectively, and the black and red shaded areas correspond to the electron parts of the DOS $[\rho^<(\omega)]$ before and after pumping, respectively. The dotted lines denote the Fermi level before pumping. (c) and (d) One-particle excitation spectra $A^>(\boldsymbol{k},\omega)$ (solid lines) and $A^<(\boldsymbol{k},\omega)$ (dotted lines) before pumping, and (e) and (f) those after pumping for $r_t = 1$. A finite size cluster of $N = 12$ sites with an open boundary condition is adopted. The parameter value is chosen to be $U/t = 6$.

where the pair-field operator is given by

$$\Delta_i = c_{i2\downarrow}c_{i1\uparrow} - c_{i2\uparrow}c_{i1\downarrow}. \tag{14}$$

This function measures the correlation between the carrier pairs created at sites j and annihilated at i. Previous calculations [29,30,32] have shown that the pair correlations at zero temperature are damped within a few sites at half filling, and are long-ranged in the doped cases. This is confirmed in the present calculation (see the regions of $\tau \ll 0$ in Fig. 8), where $P(|i-j|=1)$ is only dominant at $x_h = 0$ and $P(|i-j| \geqslant 3)$ increases with hole doping. After pumping at half filling [see the regions of $\tau > 0$ in Fig. 8(a)], $P(|i-j|=1)$ is reduced slightly and $P(|i-j| \geqslant 3)$ exhibits oscillatory behaviors with large amplitude. Away from the half filling presented in Figs. 8(b) and 8(c), the $P(|i-j|)$ for all distances decrease monotonically in response to photon pumping, while the oscillatory behaviors observed at $x_h = 0$ are weak. The reductions in $P(|i-j|)$ are not pronounced in the case of small $r_t = t'/t$, as shown in Figs. 8(d). These results can be summarized as indicating that (i) coherent oscillations of the carrier pairs are induced by the photon pumping at half filling, and (ii) the pair correlations with $|i-j| \geqslant 3$ almost disappear following the photon pumping of the hole-doped cases. Based on these results, optical control of the carrier pair coherence is demonstrated in Sec. III B.

B. Double-pulse pumping

In this section, we demonstrate the electronic state changes induced by double-pulse pumping, where two photon pulses are introduced with a time interval in the two-leg ladder Hubbard model. The vector potential for the double-pulse pumping is given by

$$A_p(\tau) = A_1 e^{-\tau^2/(2\gamma_1^2)} \cos\omega_1\tau + A_2 e^{-(\tau-\tau_d)^2/(2\gamma_2^2)} \cos\omega_2\tau, \tag{15}$$

where τ_d is the time interval between the first and second pulses, and $A_{1(2)}$, $\omega_{1(2)}$, and $\gamma_{1(2)}$ are the amplitude, frequency, and the damping factor for the first (second) pulse, respectively.

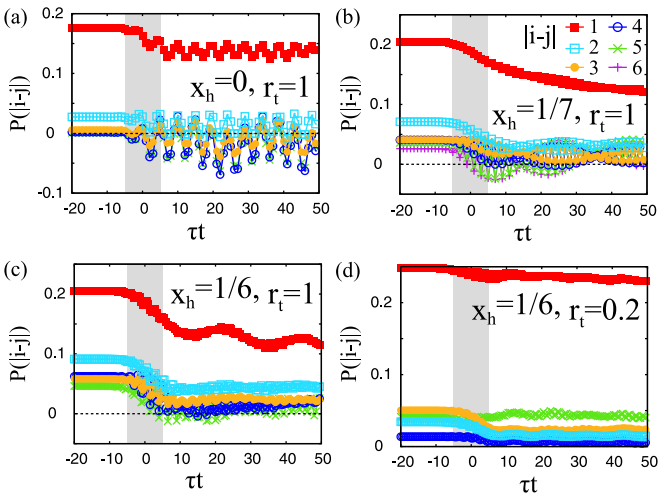

FIG. 8. Time dependences of pair-field correlation functions for several distances $|i-j|$. The hole densities are (a) $x_h = 0$, (b) 1/7, and (c) 1/6. A finite size clusters of $N = 12$ and 14 sites with an open boundary condition are adopted. The parameter values are chosen to be $U/t = 6$ and $t'/t = 1$. The results at $x_h = 1/6$ and $r_t = 0.2$ are shown in (d). The shaded area represents the time intervals at which the pump pulses are introduced.

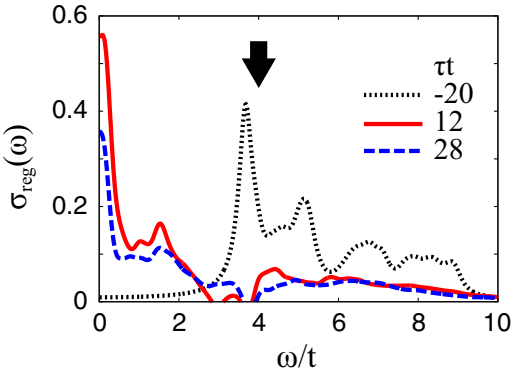

FIG. 9. Optical conductivity spectra in double-pulse pumping at half filling ($x_h = 0$). The dotted, solid, and dashed lines represent the spectra before pumping ($\tau t = -20$), between the first and second pulse pumpings ($\tau t = 12$), and after the second pulse pumping ($\tau t = 28$), respectively. A finite size cluster of $N = 12$ sites with an open boundary condition is adopted. The parameter values are chosen to be $U/t = 6$, $t'/t = 1$, $A_1 = A_2 = 0.6$, $\omega_1 = \omega_2 = 4$, and $\tau_d = 15$. The bold arrow represents the energy of the first and second photon pulses.

In the following calculations, we take $\gamma_1 = \gamma_2 = 1/t$. The photon energies in both the first and second pulses are chosen to be the optical gap energy at $x_h = 0$ before the first pumping, as $\omega_1 = \omega_2 = 4t$.

The optical conductivity spectra at half filling before the first pulse, between the first and second pulses, and after the second pulse are shown in Fig. 9. Following introduction of the first pump pulse, the D appears inside the optical gap. After the second pump pulse, reduction of the D occurs. In brief, this is a sequential change of the electronic structures, where a Mott insulator $\rightarrow$ a metallic-like state $\rightarrow$ a suppression of the metallic character. In this sense, the photodoped carriers induced by the first pump pulse play similar roles to the chemically doped carriers.

We calculate D as functions of time and show the results in Fig. 10(a), in which A_1 are varied and A_2 is fixed. The D induced by the first pulse increases with increasing A_1. On the other hand, the second pulse induces non-monotonic changes in D; when A_1 is small (large), the second pulse increases (decreases) D. The n_p and E_U are shown in Figs. 10(b) and 10(c), respectively. Not only the first pulse pumping, but also the second pulse pumping induces increases in both n_p and E_U, in contrast to the D results shown in Fig. 10(a). This implies that, even in the case of large A_1, the second pumping realizes a higher energy-excited state than the state before the second pumping, but suppresses the low-energy carrier motion. In Fig. 10(d), we show the $D(\tau)$ in the case of large A_1, where the time interval between the first and second pulses is varied. The characteristic reduction of D after the second pumping is commonly observed in all cases of τ_d. Thus, the observed phenomena are not due to the interference effects between the first and second pulse excitations.

The pairing characteristics under the influence of double-pulse pumping are examined. The time dependences of the pair-field correlation functions, $P(|i-j|)$, for $|i-j| = 1$, 3, and 5 at half filling are plotted in Fig. 11(a). Before the

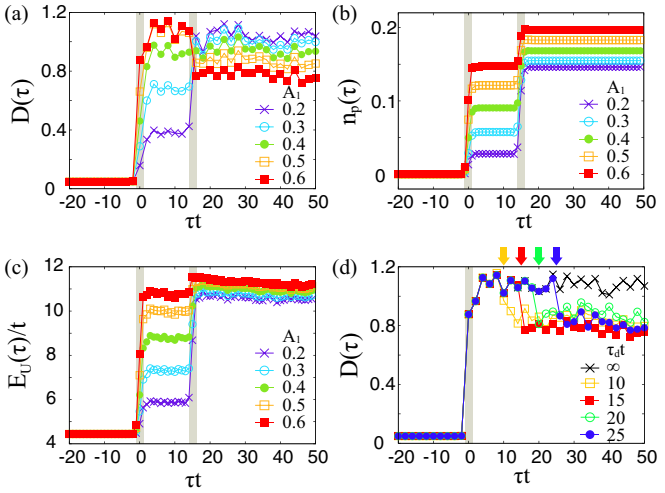

FIG. 10. Calculated results for double-pulse pumping at half filling. (a) Low-energy weights of optical conductivity spectra, (b) absorbed photon density, and (c) Coulomb interaction energy. The first pulse amplitudes are varied in the range $A_1 = 0.2$–0.6, and the second pulse amplitude is fixed to $A_2 = 0.6$. (d) Low-energy weights of optical conductivity spectra for several values of τ_d. The first and second pulse amplitudes are fixed to a $A_1 = A_2 = 0.6$. A finite size cluster of $N = 12$ sites with an open boundary condition is adopted. The parameter values are chosen to be $U/t = 6$ and $t'/t = 1$. The shaded areas represent the time intervals at which the two pump pulses are introduced.

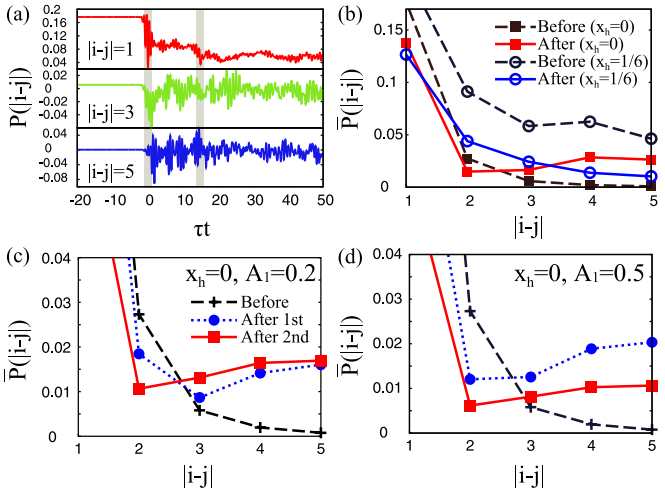

FIG. 11. (a) Time dependences of pair-field correlation functions in double-pulse pumping at half filling. The upper, middle, and lower panels show $P(|i-j|)$ for $|i-j| = 1$, 3, and 5, respectively. (b) Time-averaged pair-field correlation functions in single-pulse pumping at half filling ($x_h = 0$) and for the hole-doped case ($x_h = 1/6$). The dashed and solid lines represent $\bar{P}(|i-j|)$ before and after the photon pumpings, respectively. (c) and (d) Time-averaged pair-field correlation functions in double-pulse pumping at half filling. The first pulse amplitudes are taken to be $A_1 = 0.2$ in (c) and $A_1 = 0.5$ in (a) and (d). The second pulse amplitude is $A_2 = 0.6$ in (a), (c), and (d). The dashed, dotted, and solid lines represent $\bar{P}(|i-j|)$ before the first pulse, between the first and second pulses, and after the second pulse, respectively. A finite size cluster of $N = 12$ sites with an open boundary condition is adopted. The parameter values are chosen to be $U/t = 6$ and $t'/t = 1$.

first pulse, $P(|i-j|>3)$ is less than 5% of $P(|i-j|=1)$. After the first pulse pumping, coherent oscillations appear in $P(|i-j|)$ for all $|i-j|$, and the maximum amplitudes of the oscillations are larger than 10% of $P(|i-j|=1)$ before the first pumping. After the second pulse pumping, suppressions of the oscillation amplitudes are remarkably seen in $P(|i-j|)$ for $|i-j|=5$.

We analyze this characteristic change in the pair-field correlation function by introducing an averaged absolute value of $P(|i-j|)$ after the first and second pulse pumpings, which is defined by

$$\bar{P}(|i-j|)=\frac{1}{\Delta t}\int_{t_0}^{t_0+\Delta t} dt\,|P(|i-j|)|, \qquad (16)$$

where the parameters $(t_0,\Delta t)$ are chosen to be $(0,15)$ after the first pulse, and $(15,35)$ after the second pulse. The results for the large and small A_1's are shown in Figs. 11(c) and 11(d), respectively. For comparison, we show the calculated results for single-pulse pumping at $x_h=0$ and $1/6$ in Fig. 11(b), where we take $(t_0,\Delta t)=(15,35)$. After the first pulse pumping [see the blue dotted lines in Figs. 11(c) and 11(d)], the $\bar{P}(|i-j|)$ for $|i-j|\geqslant 3$ are enhanced. These results are qualitatively similar to that in the single pumping case at $x_h=0$ indicated by the red line in Fig. 11(b). The stronger the first pump amplitudes, the larger the change in $\bar{P}(|i-j|)$. The results after the second pulse pumping are qualitatively different for the cases with the large and small A_1's; the $\bar{P}(|i-j|)$ with $|i-j|\geqslant 3$ increase in the small A_1 case, but decrease for large A_1. In short, the second pulse promotes pair correlation in the small A_1 case, while it suppresses pair coherence in the large A_1 case. This change in $\bar{P}(|i-j|)$ for the second pulse pumping in the large A_1 case is similar to that induced by the single pumping in the hole-doped case, as shown in Fig. 11(b), where the pair correlation is shortened via pumping. These results suggest that some similarity exists between the chemically doped and photodoped hole carriers.

IV. DISCUSSION AND SUMMARY

In this section, we discuss the relationship between the present theoretical calculations and the recent optical pump-pulse experiments in the ladder cuprates. The photoinduced electronic state transition has been observed using time-resolved optical spectroscopy in insulating $Sr_{14}Cu_{24}O_{41}$, in which the nominal valence of Cu ion is +2.25 and 0.25 holes exist per Cu ion [37]. The insulating nature confirmed from the transport and optical measurements is attributable to the hole-carrier localization in the charge-density wave state. The pump-pulse energy was tuned around the insulating gap energy (1.58 eV). After the photon pumping, Drude-like metallic reflectivity appeared within 1 ps and was maintained for more than 50 ps. The photoinduced metallic reflectivity increased with increasing pump-photon fluence. These results are attributable to the photo-doping carriers and collapse of the carrier localization. Similar photoinduced transitions from an insulating state to a metallic state have been widely confirmed via experimental analyses of correlated insulating states [7–14], such as La_2CuO_4. Photoinduced emergence of a metallic feature is demonstrated in the present calculations, although the carrier concentration is set to $x_h=0$, which is different from that of $Sr_{14}Cu_{24}O_{41}$. As shown in Fig. 5(a), immediately after the photon-pulse pumping, the D appears inside the insulating gap, which produces the metallic reflectivity spectra. This characteristic photoinduced change of the electronic structure in the insulating state is insensitive to the anisotropy in the transfer integrals (r_t), as shown in Figs. 4(a) and 4(d), and may be common to a wide class of insulating states realized by electronic interactions [18,20,23,55]. It is thought that the interladder coupling, which is not considered in the present model, stabilizes the charge-density wave state in the insulating $Sr_{14}Cu_{24}O_{41}$. This coupling may also enhance the Mott insulating character of the present initial state, and may tend to quantitatively suppress the photoinduced metallic character.

Time-resolved optical experiments have also been performed for metallic ladder cuprates, $Sr_{14-x}Ca_xCu_{24}O_{41}$ with $x=10$ [38,39]. The pump-photon energy was tuned to 1.58 eV, corresponding to the charge-transfer excitation energy in the ladder plane. Immediately after the photon pumping, the low-energy optical reflectivity at 0.5 eV exhibited a reduction, which implies suppression of the initial metallic character. The experimental reflectivity exhibited a slow increase after approximately 0.5 ps, which was interpreted as thermalization through the lattice degrees of freedom. The present theoretical calculations provide a possible interpretation for this experimental observation of the photoinduced suppression of the metallic state. This photoinduced suppression is confirmed not only through calculations of the pump-probe spectra, but also using the calculations of the low-energy component of the kinetic energy, the one-particle excitation spectra, and other characteristics. As shown in Figs. 4(b)–4(f), we reveal that the ladder lattice effect plays an essential role in this suppression, in contrast to the photoinduced emergence of a metallic feature in the Mott insulating state. It has been reported experimentally that the transient suppression of the initial metallic character by photon pumping barely reflects the temperature dependence. Thus, we expect that the present calculations at zero temperature are applicable to the interpretation of the experimental observations reported in Refs. [38,39].

The double-pulse pumping case reinforces the validity of the present scenario for the photoexcited state in metallic ladder cuprates. Time-resolved spectroscopy under double-pulse pumping has been performed experimentally in insulating $Sr_{14}Cu_{24}O_{41}$ [39]. The first pump-pulse fluence was varied and the second pulse fluence was fixed, similar to the present theoretical calculation introduced in Sec. III B. Increases in the reflectivity at 0.5 eV were observed monotonically as functions of the first pulse fluence. On the other hand, the change in the reflectivity induced by the second pulse pumping was qualitatively dependent on the first pulse fluence; the reflectivity within 0.5 ps after the second pulse pumping increased (decreased) for the weak (strong) first pulse fluence. This reflectivity variation behavior is well reproduced qualitatively by the present calculations, as shown in Fig. 9. Note that, in the experiments, the reflectivity began to increase over 0.5 ps after the second pulse pumping, being independent of the second pulse fluence. This is attributable to the relaxation to the other degrees of freedom, which are not considered in the present theoretical calculations.

In conclusion, we have studied photoinduced carrier dynamics in a correlated electron system on a two-leg ladder lattice. The ladder Hubbard model was analyzed utilizing the numerical exact diagonalization method in finite size clusters, based on the Lanczos algorithm. Through calculations of the transient low-energy kinetic energy, optical conductivity spectra, one-particle excitation spectra, and other characteristics, we found that the initial metallic state is suppressed by the photon-pulse pumping. This is in contrast to the photoinduced metallic state in the Mott insulating state. The ladder lattice effect plays an essential role in this photoinduced suppression of the metallic character. Calculations for the double-pulse pumping case and comparisons with the corresponding pump-probe experiments confirm the nature of the characteristic photoinduced excited states in this correlated electron system on a two-leg ladder lattice.

ACKNOWLEDGMENTS

We thank S. Koshihara, Y. Okimoto, R. Fukaya, M. Naka, and J. Nasu for their helpful discussions. This work was supported by MEXT KAKENHI Grants No. 26287070 and No. 15H02100. Some of the numerical calculations were performed using the facilities of the Supercomputer Center, the Institute for Solid State Physics, the University of Tokyo.

[1] *Photo-Induced Phase Transitions*, edited by K. Nasu (World Scientific, New Jersey, 2004).
[2] *Photo-Induced Phase Transitions and Their Dynamics*, edited by M. Kuwata-Gonokami and S. Koshihara, special topics of J. Phys. Soc. Jpn. **75**, 011001 (2006).
[3] K. Miyasaka, M. Nakamura, Y. Ogimoto, H. Tamaru, and K. Miyano, Phys. Rev. B **74**, 012401 (2006).
[4] H. Ehrke, R. I. Tobey, S. Wall, S. A. Cavill, M. Först, V. Khanna, Th. Garl, N. Stojanovic, D. Prabhakaran, A. T. Boothroyd, M. Gensch, A. Mirone, P. Reutler, A. Revcolevschi, S. S. Dhesi, and A. Cavalleri, Phys. Rev. Lett. **106**, 217401 (2011).
[5] H. Uemura and H. Okamoto, Phys. Rev. Lett. **105**, 258302 (2010).
[6] T. Miyamoto, K. Kimura, T. Hamamoto, H. Uemura, H. Yada, H. Matsuzaki, S. Horiuchi, and H. Okamoto, Phys. Rev. Lett. **111**, 187801 (2013).
[7] T. Ogasawara, M. Ashida, N. Motoyama, H. Eisaki, S. Uchida, Y. Tokura, H. Ghosh, A. Shukla, S. Mazumdar, and M. Kuwata-Gonokami, Phys. Rev. Lett. **85**, 2204 (2000).
[8] S. Iwai, M. Ono, A. Maeda, H. Matsuzaki, H. Kishida, H. Okamoto, and Y. Tokura, Phys. Rev. Lett. **91**, 057401 (2003).
[9] H. Okamoto, H. Matsuzaki, T. Wakabayashi, Y. Takahashi, and T. Hasegawa, Phys. Rev. Lett. **98**, 037401 (2007).
[10] H. Okamoto, T. Miyagoe, K. Kobayashi, H. Uemura, H. Nishioka, H. Matsuzaki, A. Sawa, and Y. Tokura, Phys. Rev. B **82**, 060513(R) (2010).
[11] H. Okamoto, T. Miyagoe, K. Kobayashi, H. Uemura, H. Nishioka, H. Matsuzaki, A. Sawa, and Y. Tokura, Phys. Rev. B **83**, 125102 (2011).
[12] H. Matsuzaki, M. Iwata, T. Miyamoto, T. Terashige, K. Iwano, S. Takaishi, M. Takamura, S. Kumagai, M. Yamashita, R. Takahashi, Y. Wakabayashi, and H. Okamoto, Phys. Rev. Lett. **113**, 096403 (2014).
[13] N. Tajima, J. Fujisawa, N. Naka, T. Ishihara, R. Kato, Y. Nishio, and K. Kajita, J. Phys. Soc. Jpn. **74**, 511 (2005).
[14] Y. Kawakami, T. Fukatsu, Y. Sakurai, H. Unno, H. Itoh, S. Iwai, T. Sasaki, K. Yamamoto, K. Yakushi, and K. Yonemitsu, Phys. Rev. Lett. **105**, 246402 (2010).
[15] D. Fausti, R. I. Tobey, N. Dean, S. Kaiser, A. Dienst, M. C. Hoffmann, S. Pyon, T. Takayama, H. Takagi, and A. Cavalleri, Science **331**, 189 (2011).
[16] D. Nicoletti, E. Casandruc, Y. Laplace, V. Khanna, C. R. Hunt, S. Kaiser, S. S. Dhesi, G. D. Gu, J. P. Hill, and A. Cavalleri, Phys. Rev. B **90**, 100503 (2014).
[17] B. Mansart, J. Lorenzana, A. Mann, A. Odeh, M. Scarongella, M. Chergui, and F. Carbone, Proc. Natl. Acad. Sci. USA **110**, 4539 (2013).
[18] E. Iyoda and S. Ishihara, Phys. Rev. B **89**, 125126 (2014).
[19] Z. Lenarčič and P. Prelovšek, Phys. Rev. Lett. **111**, 016401 (2013).
[20] N. Maeshima and K. Yonemitsu, J. Phys. Soc. Jpn. **74**, 2671 (2005).
[21] Z. Lenarčič, D. Golež, J. Bonča, and P. Prelovšek, Phys. Rev. B **89**, 125123 (2014).
[22] H. Lu, S. Sota, H. Matsueda, J. Bonča, and T. Tohyama, Phys. Rev. Lett. **109**, 197401 (2012).
[23] H. Lu, C. Shao, J. Bonča, D. Manske, and T. Tohyama, Phys. Rev. B **91**, 245117 (2015).
[24] T. Nagata, M. Uehara, J. Goto, J. Akimitsu, N. Motoyama, H. Eisaki, S. Uchida, H. Takahashi, T. Nakanishi, and N. Mori, Phys. Rev. Lett. **81**, 1090 (1998).
[25] N. Motoyama, H. Eisaki, S. Uchida, N. Takeshita, N. Mori, T. Nakanishi, and H. Takahashi, Europhys. Lett. **58**, 758 (2002).
[26] M. Uehara, T. Nagata, J. Akimitsu, H. Takahashi, N. Mori, and K. Kinoshita, J. Phys. Soc. Jpn. **65**, 2764 (1996).
[27] T. Osafune, N. Motoyama, H. Eisaki, and S. Uchida, Phys. Rev. Lett. **78**, 1980 (1997).
[28] E. Dagotto and T. M. Rice, Science, **271**, 618 (1996).
[29] R. M. Noack, S. R. White, and D. J. Scalapino, Phys. Rev. Lett. **73**, 882 (1994).
[30] R. M. Noack, S. R. White, and D. J. Scalapino, Physica C **270**, 281 (1996).
[31] J. Riera, D. Poilblanc, and E. Dagotto, Eur. Phys. J. B **7**, 53 (1999).
[32] E. Dagotto, J. Riera, and D. Scalapino, Phys. Rev. B **45**, 5744 (1992).
[33] H. Tsunetsugu, M. Troyer, and T. M. Rice, Phys. Rev. B **49**, 16078 (1994).
[34] L. G. G. V. Dias da Silva, G. Alvarez, and E. Dagotto, Phys. Rev. B **86**, 195103 (2012).
[35] M. Mierzejewski, L. Vidmar, J. Bonča, and P. Prelovšek, Phys. Rev. Lett. **106**, 196401 (2011).
[36] J. Bonča, M. Mierzejewski, and L. Vidmar, Phys. Rev. Lett. **109**, 156404 (2012).
[37] R. Fukaya, Y. Okimoto, M. Kunitomo, T. Ishikawa, K. Onda, S. Koshihara, A. Isayama, and T. Sasagawa, J. Phys. Soc. Jpn. **82**, 083707 (2013).

[38] R. Fukaya, M. Kunitomo, Y. Okimoto, T. Ishikawa, K. Onda, S. Koshihara, H. Yui, and T. Sasagawa, Acta Phys. Pol. A, **121**, 310 (2012).
[39] R. Fukaya, Y. Okimoto, M. Kunitomo, K. Onda, T. Ishikawa, S. Koshihara, H. Hashimoto, S. Ishihara, A. Isayama, H. Yui, and T. Sasagawa, Nat. Commun. **6**, 8519 (2015).
[40] T. Dahm and D. J. Scalapino, Physica C **288**, 33 (1997).
[41] R. M. Noack, S. R. White, and D. J. Scalapino, Europhys. Lett. **30**, 163 (1995).
[42] L. Balents and M. P. A. Fisher, Phys. Rev. B **53**, 12133 (1996).
[43] H. Endres, R. M. Noack, W. Hanke, D. Poilblanc, and D. J. Scalapino, Phys. Rev. B **53**, 5530 (1996).
[44] J. Kishine and K. Yonemitsu, J. Phys. Soc. Jpn. **67**, 1714 (1998).
[45] Z. Weihong, J. Oitmaa, C. J. Hamer, and R. J. Bursill, J. Phys.: Condens. Matter **13**, 433 (2001).
[46] T. J. Park and J. C. Light, J. Chem. Phys. **85**, 5870 (1986).
[47] P. Prelovsek and J. Bonca, *Strongly Correlated Systems*, edited by A. Avella and F. Mancini (Springer, Berlin, 2013).
[48] H. Yokoyama, M. Ogata, Y. Tanaka, K. Kobayashi, and H. Tsuchiura, J. Phys. Soc. Jpn. **82**, 014707 (2013).
[49] N. Strohmaier, D. Greif, R. Jordens, L. Tarruell, H. Moritz, T. Esslinger, R. Sensarma, D. Pekker, E. Altman, and E. Demler, Phys. Rev. Lett. **104**, 080401 (2010).
[50] G. De Filippis, V. Cataudella, E. A. Nowadnick, T. P. Devereaux, A. S. Mishchenko, and N. Nagaosa, Phys. Rev. Lett. **109**, 176402 (2012).
[51] Y. Kanamori, H. Matsueda, and S. Ishihara, Phys. Rev. B **82**, 115101 (2010).
[52] J. Ohara, Y. Kanamori, and S. Ishihara, Phys. Rev. B **88**, 085107 (2013).
[53] J. Wagner, W. Hanke, and D. J. Scalapino, Phys. Rev. B **43**, 10517 (1991).
[54] A. Shimizu and T. Yuge, J. Phys. Soc. Jpn. **80**, 093706 (2011).
[55] M. Eckstein and P. Werner, Phys. Rev. Lett. **110**, 126401 (2013).